Zwitterionic Ferrocenes: An Approach for Redox Flow Battery (RFB) Catholytes

Baosen Zhang; Briana R. Schrage, Ariana Frkonja-Kuczin, Sanjay Gaire, Ivan A. Popov,* Christopher J. Ziegler,* and Aliaksei Boika*

Department of Chemistry, University of Akron, Akron OH 44325-3601, USA.

* Corresponding Authors

Aliaksei Boika, E-mail: aboika@uakron.edu; Ivan A. Popov, E-mail: ipopov@uakron.edu; Christopher J.

Ziegler, E-mail: <u>ziegler@uakron.edu</u>

ABSTRACT

Herein we present two new ferrocene compounds with zwitterionic side chains, propyl (Fc3) and butyl (Fc4). These compounds are highly soluble in water (0.66 M for Fc3 and 2.01 M for Fc4). When paired with anthraquinone-2,7-disulfonate as the anolyte, these zwitterionic ferrocenes exhibit excellent performance under neutral aqueous conditions. Voltage and energy efficiencies were ca. 88 %, and coulombic efficiency was over 99% for both high concentration RFBs. We did observe a difference in stability between the lengths of the zwitterionic chains, with Fc4 showing higher stability than Fc3, and the capacity decrease by ~5% at the end of 20 cycles (~1% per day). DFT calculations revealed striking differences in the conformational properties between Fc3 and Fc4, with Fc4 retaining a linear structure of the side chain in solution while Fc3 favouring both linear and curved geometries.

Interest in redox flow batteries (RFBs) has increased due to their promise of superior performance in energy storage and for their potential solution to the issues of discontinuity and intermittency of renewable energy sources like wind and solar energy. Since the two electrolytes in RFBs are stored in separate tanks, this design exhibits numerous advantages when compared with other energy storage technologies. PFBs can be classified by their solvent systems, which comprise aqueous RFBs (ARFBs) and non-aqueous RFBs. In general, when compared with non-aqueous RFB designs, ARFB devices possess advantages such as lower electrolyte resistance, lower costs, improved safety, and improved environmental-friendliness. Recently, the study of ferrocene-based ARFBs has increased due to their stable and reversible redox reactions. In this report we present two new ferrocenes that incorporate a zwitterionic structure at the periphery. These compounds exhibit low capacity drops due to their high stabilities while maintaining high solubilities required for optimal energy density. This is the first time that a zwitterionic ferrocene has been utilized in an ARFB system under neutral pH conditions.

Ferrocene can be readily modified by adding functional groups to the cyclopentadienyl (Cp) ring, which make the resultant ferrocene derivatives highly soluble in water. We recently successfully presented an aqueous battery system that paired ferrocene bis sulfonate salts with disodium anthraquinone-2,7-disulfonate salt (AQDS). One major challenge for these battery systems is the capacity drop during cycling due to the decomposition of ferrocene compounds. To address this we successfully synthesized a new pair of zwitterionic ferrocenes with propyl (3-((ferrocen-yl))methyldimethylammonio)-1-

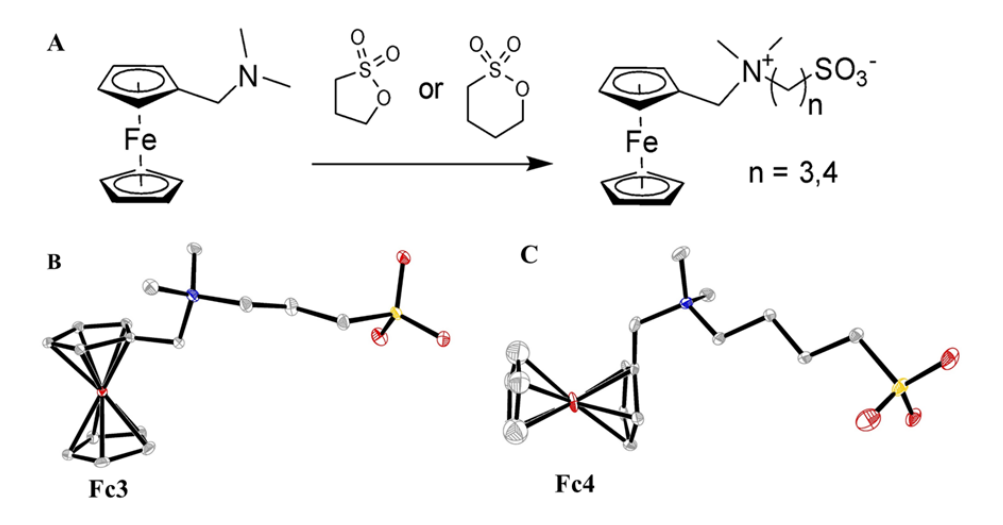


Figure 1. The synthesis **(A)** and single crystal X-ray structures of zwitterionic ferrocenes **Fc3 (B)** and **Fc4 (C)** with 35% thermal ellipsoids. Hydrogen atoms and solvent waters are omitted for clarity.

propanesulfonate, **Fc3**) and butyl (4-((ferrocen-yl)methyldimethylammonio)-1-butanesulfonate, **Fc4**) chains. These compounds are prepared by reaction of the propyl and butyl sultone, respectively, with dimethylaminomethylferrocene as shown in Figure 1. The resultant products are isolated in good yield as pure crystalline materials. The structures are highly similar, with the exception of the orientation of the alkyl chain (Figures S7, S8). These two compounds are highly miscible with water, with solubilities of 0.66 and 2.01 M, for **Fc3** and **Fc4**, respectively. Based on the solubility, the theoretical volumetric capacity can be calculated using Faraday's law, which results in the values of 17.69 Ah/L and 53.87 Ah/L.

The cyclic voltammograms (CVs) of **Fc3** and **Fc4** are shown in Figure S9, which reveal highly reversible redox processes. The half-wave potential for **Fc3** and **Fc4** are 0.456 V and 0.453 V, respectively, in 1 M NaNO₃ as a supporting electrolyte (reference electrode Ag|AgCl|KCl (2M)). Pairing with AQDS, the **Fc3**/AQDS ARFB device has an open circuit voltage (OCP) of 0.915 V and **Fc4**/AQDS ARFB device has the OCP value of 0.913 V (Figure S10). From these numbers, the theoretical energy density was calculated to be 16.18 Wh/L for **Fc3** RFB and 49.18 Wh/L for Fc4 RFB. The CVs were studied at different scan rates and the scan rate dependence of **Fc3** and **Fc4** demonstrate they are diffusion-controlled processes (Figure S9). The diffusion coefficients for both compounds were evaluated by the Randles-Sevcik equation and

obtained values were 5.58·10⁻⁶ for **Fc3** and 3.38·10⁻⁶ cm²/s for **Fc4**, comparable with the ones published previously for ferrocene sulfonate salts.^{10,11} The electrochemical data for **Fc3** and **Fc4** are summarized in Table S2.

The zwitterionic compounds Fc3 and Fc4 were initially evaluated at low concentrations in a RFB device, and full battery tests were performed with 10 mL of 30 mM of the zwitterionic ferrocenes as the catholytes and 30 mL of 30 mM AQDS as the anolyte. In both cases, an excess of AQDS was used to make the ferrocene side capacity limiting. The catholytic and anolytic chambers both used 1 M NaNO₃ as the supporting electrolyte. The battery was charged and discharged at 2.5 mA/cm² from 0 V to 1.2 V and the charge-discharge curves, capacity and efficiency versus the cycle number are shown in Figure S11 and Figure S12. Fc3/AQDS ARFB gave an energy efficiency (EE) and voltage efficiency (VE) of ~80% and a coulombic efficiency (CE) of over 99% at the end of 100 cycles, while Fc4/AQDS RFB gave an EE and VE of ~80% and a CE of over 99% at the end of 100 cycles. The capacity loss is observed for Fc3/AQDS RFB because of the decomposition of Fc3; an extra peak shows up in the post-cycling CV analysis (Figure S13 A). However, compared to Fc3/AQDS ARFB, little capacity loss was observed for the Fc4/AQDS ARFB. The post-cycling CV analysis also keeps consistent with this observation (see Figure S13 B). This obvious increase in stability is the difference in alkyl chain length between the two compounds.

Compounds **Fc3** and **Fc4** were then evaluated at the higher concentration of 0.3 M (10 mL). The anolyte was 30 mL of 0.1 M AQDS, and the supporting electrolyte was still 1 M NaNO₃. The charge and discharge cycles were tested with cutoff voltages at 1.2 V for the charge process and 0 V for the discharge process at a current density of 2.5 mA/cm². The charge-discharge cycling results are shown in Figure 2, and the charge and discharge capacity and efficiency are also shown in the same figure. The **Fc3**/AQDS RFB gave an EE of ~88% initially and became stable at ~84% and a CE of over 99% at the end of 20 cycles. **Fc4**/AQDS RFB gave an EE of ~90% and became stable at ~88% and a CE of over 99%. For **Fc3**, the discharge capacity

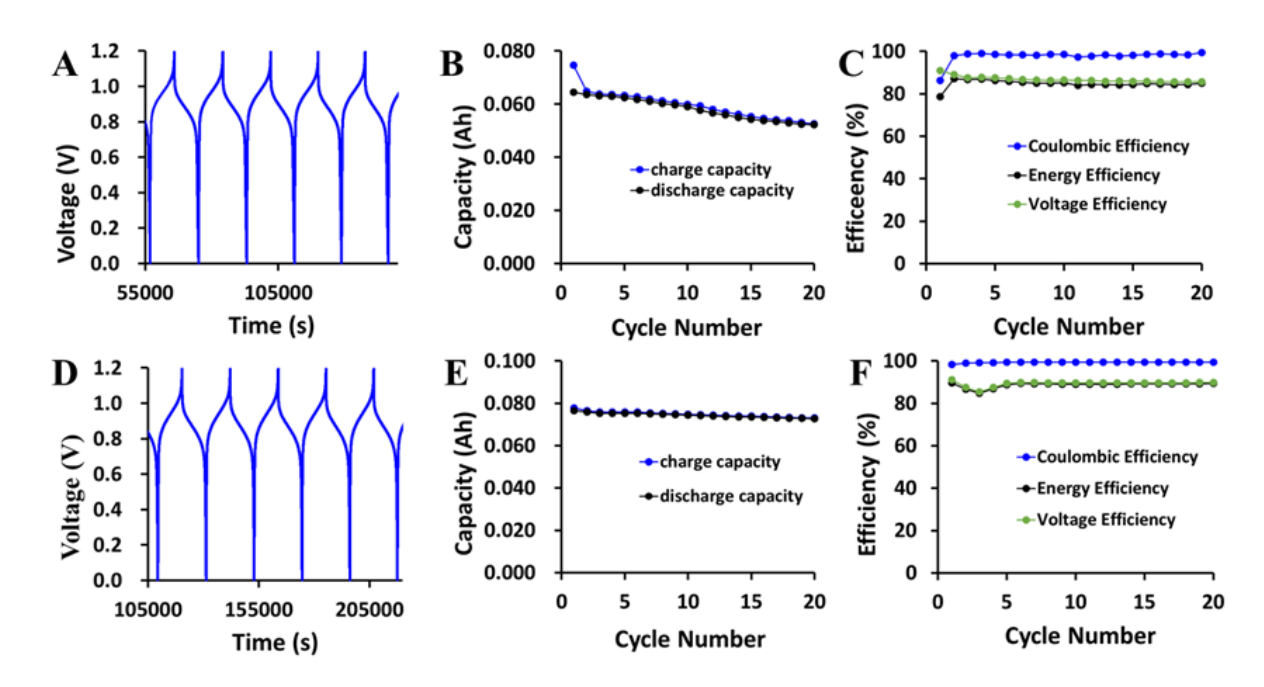


Figure 2. (**A**) Charge-discharge curve (cycle# 3-7); (**B**) the charge and discharge capacity over 20 cycles; (**C**) EE, CE, and VE for **Fc3**/AQDS RFB. (**D**) charge-discharge curve (cycle# 6-10); (**E**) the charge and discharge capacity over 20 cycles; (**F**) EE, CE, and VE for **Fc4**/AQDS RFB. The concentration of catholyte was 0.3 M and the supporting electrolyte was 1 M NaNO₃.

dropped ~15% at the end of 20 cycles (~3% capacity drop per day), while the **Fc4** dropped ~5% at the end of 20 cycles (~1% capacity drop per day). Once again, **Fc4** exhibits a higher stability than **Fc3**. The small capacity drop in the **Fc4** cell mainly results from the crossover of **Fc4** to the anodic compartment (~1.7%, Figure S15), as well as the other losses of **Fc4** in the cathodic compartment (~3.3%), such as a small amount of leakage from the cell and adherence to the membrane (Figure S16).

Figure S14 shows the current rate performance that was studied from 2.5 to 10 mA/cm² with increments of 2.5 mA/cm². Flow cell tests were conducted with concentration of 0.3 M (10 mL) of zwitterionic compounds as the positive electrolyte and 0.1 M AQDS (30mL) as the negative electrolyte. The supporting electrolyte was 3 M NaNO₃ for both compartments. The charge-discharge process was investigated under the same conditions as the higher concentration RFB. The observed trends of capacity decrease with current density are attributed to high cell resistance. Representative charge/discharge profiles of the Fc3/AQDS and Fc4/AQDS ARFB are shown in Figure S14B and S14E. The trend of EE for the

0.3 M Fc3/AQDS and 0.3 M Fc4/AQDS ARFB are outlined in Figures S14C and S14F. EE decreased from 88% for 2.5 mA/cm² to 57% for 10 mA/cm² for Fc3. The EE decreased from 88% for 2.5 mA/cm² to 63% for 10 mA/cm² for Fc4. The trends observed for the energy efficiency are typical and explained by the increased cell overpotential at higher current densities. The EE drops quickly with the current density increase. Fc3 or Fc4 might adhere to the Nafion 117 membrane, which causes a decrease of the membrane conductivity. This is evident from Figure S16 for Nafion 117 membrane and the results for Fumasep FAA-3-50 anion exchange membrane (Figures S17 and S18). Therefore, zwitterionic-based RFB design could be improved with better membranes.

Subsequently, density functional theory (DFT) calculations were performed to investigate the stability of possible conformations of the two zwitterionic ferrocenes. The calculations were based on the assessment of thermodynamic and kinetic factors contributing to the stability of plausible conformational structures of Fc3 and Fc4 present in an aqueous solution (Figures S22-S25). Combining DFT calculations and implicit solvation models¹⁵ to predict redox potentials for molecular systems has become standard protocol, and this was also employed successfully in our recent studies of Fe-complexes¹⁶⁻¹⁸ (see Supporting Information for computational details). Since Fc3 and Fc4 differ in the orientation of the alkyl chain (Figure S22), we computationally explored a possibility of transforming the crystal Fc3 structure into the Fc4-like geometry. As shown in Figure 3, the transformation from crystal [Fc3]⁰ to [Fc4]⁰-like isomer (named N-C+C-N) can be achieved by two routes (green and blue dashed lines) involving 2 LM (N-C, C-N) and 4 TS structures (TS2, TS2', TS3, TS3') (see Figures S26-S29 for the detailed transformation schemes of [Fc3]⁰, [Fc3]⁺, [Fc4]⁰, and [Fc4]⁺). Additionally, a transformation into one more stable isomer named 'curved' was evaluated via the TS1 barrier. Curved [Fc3]⁰ is stabilized by additional hydrogen bonding interactions due to the attraction of the negatively charged O atoms of the SO₃ moiety to the H atoms of the side chain and the Fc ring (Figure S30).

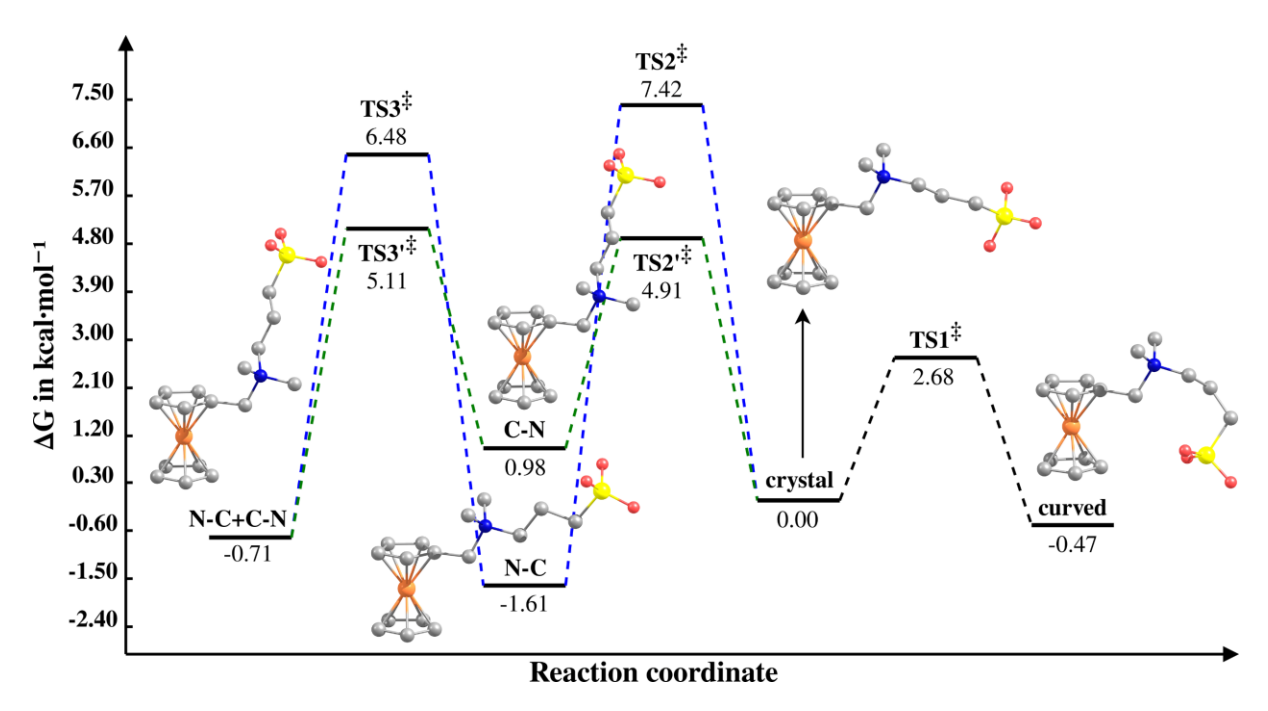


Figure 3. Schematic Gibbs free energy diagram evaluating possible transformations of the crystal structure of [Fc3]⁰ (crystal) into the [Fc4]⁰-like N-C+C-N structure and the curved structure.

Comparing the kinetic barriers related to all these transformations of the **crystal** structure of [**Fc3**]^o (Table S4), it is clear that the **crystal**-to-**curved** transformation (**TS1**) represents the most kinetically probable path due to the smallest barrier of 2.68 kcal/mol. Hence, this may indicate a possibility for the coexistence of these two structural forms of [**Fc3**]^o in an aqueous solution. Upon oxidation, the **curved** [**Fc3**]⁺ structure becomes even more thermodynamically stable and favourable than the **crystal** [**Fc3**]⁺ (by 2.56 kcal/mol), with the kinetic barrier from the **crystal** [**Fc3**]⁺ to the **curved** [**Fc3**]⁺ becoming slightly smaller than in the electroneutral counterparts, *i.e.* 2.68 vs. 2.37 kcal/mol (**TS1**, Figure S23). In contrast, similar **crystal**-to-**curved** transformations in [**Fc4**]^{0/+} species are less likely, hindered by twice larger barriers, *i.e.* 5.56-6.38 kcal/mol (Figures S24, S25, Table S5). The probable coexistence of the two isomers of **Fc3** in water agrees with the appearance of the extra set of peaks showing up in the post-cycling CV analysis (Figure S13A). The computed redox potential of the **curved Fc3** isomer (0.080 eV, vs. FcCH₂OH⁺|FcCH₂OH) shows slightly more negative value compared to that for the **crystal Fc3** structure (0.170 eV), in accordance with the experimental extra peak shifted in the same direction, *i.e.* 0.020 eV vs. 0.200 eV, respectively (Table S6).

However, it should be noted that while the conformational change may contribute to the appearance of the extra set of peaks, the major contribution is likely due to the decomposition of **Fc3**. Therefore, additional experiments are needed to investigate the nature of the decomposition product, as well as to identify possible mechanism of degradation by performing theoretical calculations. Related research is currently underway in our groups to further investigate this process from both experimental and theoretical perspectives.

In conclusion, we have prepared new zwitterionic ferrocene derivatives, Fc3 and Fc4, which have been synthesized, fully characterized, and used for the first time as catholytes in aqueous RFBs at neutral pH. AQDS was used as the anolyte, and both Fc3 and Fc4 RFB devices showed high efficiency in their operation. Interestingly, RFB capacity monitoring and cyclic voltammetry analyses revealed higher stability for the butyl derivative (Fc4) compared to propyl (Fc3). We employed DFT calculations to investigate the stability of possible conformations of the two zwitterionic ferrocenes in solution. Our calculations revealed striking differences in the conformational properties between Fc3 and Fc4, with Fc4 retaining a linear structure of the side chain in solution, and Fc3 favouring both linear and curved geometries. We believe that the approach presented here introduces a fundamentally new direction in the development of aqueous RFBs. Furthermore, a zwitterionic approach may serve as a general guideline for the design of RFBs with improved solubility and cyclability characteristics that are highly desirable for next generation batteries. We are continuing our investigations into water soluble ferrocenes as catholytic materials for RFB applications.

Associated Content

Electronic supplementary information (ESI) available: Synthetic procedures, characterization, electrochemical experiments, X-ray parameters and computational details. CCDC 2129560-2129561

contain the supplementary crystallographic data for this paper. For ESI and crystallographic data in CIF or other electronic format see DOI: XXX

Acknowledgement

The authors thank Dr. Zhiling Zhao (Institute for Bioscience & Biotechnology Research, University of Maryland, College Park) for helpful discussions. I.A.P. acknowledges the computational resources at the Ohio Supercomputer Center and the ARCC HPC cluster at the University of Akron. The authors are grateful to the University of Akron and the National Science Foundation (CHE-1665267) for support of this research.

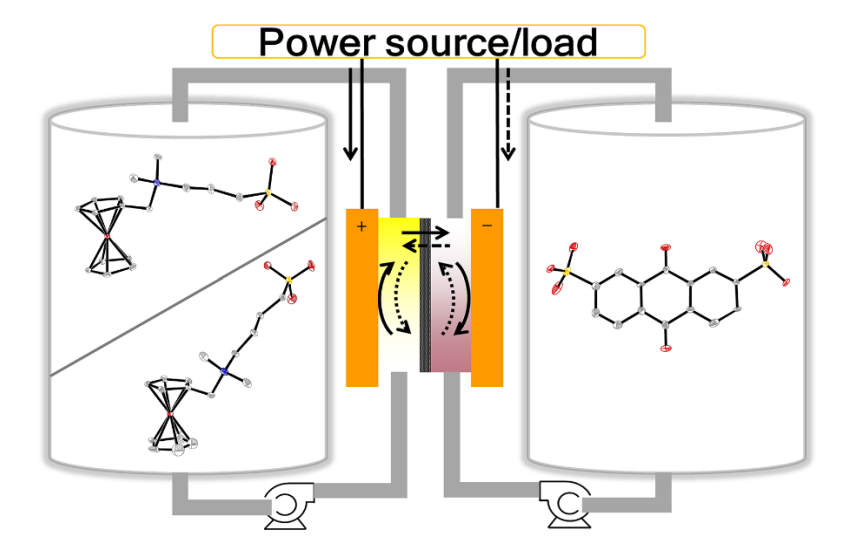
REFERENCES

- (1) Goodenough, J. B.; Park, K.-S. The Li-Ion Rechargeable Battery: A Perspective. *J. Am. Chem. Soc.* **2013**, *135* (4), 1167–1176. https://doi.org/10.1021/ja3091438.
- (2) Liu, W.; Lu, W.; Zhang, H.; Li, X. Aqueous Flow Batteries: Research and Development. *Chem. Eur. J.* **2019**, *25* (7), 1649–1664. https://doi.org/10.1002/chem.201802798.
- (3) Badwal, S. P. S.; Giddey, S. S.; Munnings, C.; Bhatt, A. I.; Hollenkamp, A. F. Emerging Electrochemical Energy Conversion and Storage Technologies. *Front. Chem.* **2014**, *2*, *79*. https://doi.org/10.3389/fchem.2014.00079.
- (4) Khaligh, A.; Li, Z. Battery, Ultracapacitor, Fuel Cell, and Hybrid Energy Storage Systems for Electric, Hybrid Electric, Fuel Cell, and Plug-In Hybrid Electric Vehicles: State of the Art. *IEEE Transactions on Vehicular Technology* **2010**, *59* (6), 2806–2814. https://doi.org/10.1109/TVT.2010.2047877.
- (5) Smith, W. The Role of Fuel Cells in Energy Storage. *Journal of Power Sources* **2000**, *86* (1), 74–83. https://doi.org/10.1016/S0378-7753(99)00485-1.

- (6) Terada, N.; Yanagi, T.; Arai, S.; Yoshikawa, M.; Ohta, K.; Nakajima, N.; Yanai, A.; Arai, N. Development of Lithium Batteries for Energy Storage and EV Applications. *Journal of Power Sources* **2001**, *100* (1), 80–92. https://doi.org/10.1016/S0378-7753(01)00885-0.
- (7) Kwabi, D. G.; Ji, Y.; Aziz, M. J. Electrolyte Lifetime in Aqueous Organic Redox Flow Batteries: A Critical Review. *Chem. Rev.* **2020**, *120* (14), 6467–6489. https://doi.org/10.1021/acs.chemrev.9b00599.
- (8) Gong, K.; Fang, Q.; Gu, S.; Li, S. F. Y.; Yan, Y. Nonaqueous Redox-Flow Batteries: Organic Solvents, Supporting Electrolytes, and Redox Pairs. *Energy Environ. Sci.* **2015**, *8* (12), 3515–3530. https://doi.org/10.1039/C5EE02341F.
- (9) Li, M.; Rhodes, Z.; Cabrera-Pardo, J. R.; Minteer, S. D. Recent Advancements in Rational Design of Non-Aqueous Organic Redox Flow Batteries. *Sustainable Energy Fuels* **2020**, *4* (9), 4370–4389. https://doi.org/10.1039/D0SE00800A.
- (10) Zhao, Z.; Zhang, B.; Schrage, B. R.; Ziegler, C. J.; Boika, A. Investigations Into Aqueous Redox Flow Batteries Based on Ferrocene Bisulfonate. *ACS Appl. Energy Mater.* **2020**, *3* (10), 10270–10277. https://doi.org/10.1021/acsaem.0c02259.
- (11) Schrage, B. R.; Zhang, B.; Petrochko, S. C.; Zhao, Z.; Frkonja-Kuczin, A.; Boika, A.; Ziegler, C. J. Highly Soluble Imidazolium Ferrocene Bis(Sulfonate) Salts for Redox Flow Battery Applications. *Inorg. Chem.* **2021**, *60* (14), 10764–10771. https://doi.org/10.1021/acs.inorgchem.1c01473.
- (12) Chen, Q.; Li, Y.; Liu, Y.; Sun, P.; Yang, Z.; Xu, T. Designer Ferrocene Catholyte for Aqueous Organic Flow Batteries. *ChemSusChem. 2021,* 14(5), 1295-1301 . https://doi.org/10.1002/cssc.202002467.
- (13) Yu, J.; Salla, M.; Zhang, H.; Ji, Y.; Zhang, F.; Zhou, M.; Wang, Q. A Robust Anionic Sulfonated Ferrocene Derivative for PH-Neutral Aqueous Flow Battery. *Energy Storage Materials* **2020**, *29*, 216–222. https://doi.org/10.1016/j.ensm.2020.04.020.

- (14) Hu, B.; DeBruler, C.; Rhodes, Z.; Liu, T. L. Long-Cycling Aqueous Organic Redox Flow Battery (AORFB) toward Sustainable and Safe Energy Storage. *J. Am. Chem. Soc.* **2017**, *139* (3), 1207–1214. https://doi.org/10.1021/jacs.6b10984.
- (15) Cramer; C. J.; Truhlar, D. G. Implicit Solvation Models: Equilibria, Structure, Spectra, and Dynamics, *Chem. Rev.* **1999**, *99*, 2161–2200.
- (16) Popov, I. A.; Mehio, N.; Smythe, N. C.; Chu, T.; Davis, B. L.; Gordon, J. C.; Mukundan, R.; Yang, P. E. R. Batista, Impact of Ligand Substitutions on Multielectron Redox Properties of Fe Complexes Supported by Nitrogenous Chelates. *ACS Omega* **2018**, *3*, 14766–14778.
- (17) Popov, I. A.; Davis, B. L.; Mukundan, R.; Batista, E. R.; Yang, P. Catalyst-Inspired Charge Carriers for High Energy Density Redox Flow Batteries. *Front. Phys.* **2019**, *6*, 1–10.
- (18) Sharma, S.; Maurya, S.; Popov, I. A.; Andrade, G. A.; Davis, B. L.; Mukundan, R.; Smythe, N. L.; Gordon, J. C.; Batista, E. R.; Yang, P. Iron-Iminopyridine Complexes as Charge Carriers for Non-Aqueous Redox Flow Battery Applications. *Energy Storage Mater.* **2021**, *37*, 576–586.

TOC GRAPHIC



TOC synopsis:

Two new ferrocene compounds with propyl (Fc3) and butyl (Fc4) zwitterionic side chains have been synthesized and fully characterized (shown on the left). These compounds have been studied electrochemically and with DFT methods, and displayed great promise as catholyte materials for redox flow battery applications.